Nanoscale

Measuring the Internal Quantum Yield of Upconversion Luminescence for Ytterbium-Sensitized Upconversion Phosphors Using the Ytterbium(III) Emission as an Internal Standard

SCHOLARONE™
Manuscripts

Measuring the Internal Quantum Yield of Upconversion Luminescence for Ytterbium-Sensitized Upconversion Phosphors Using the Ytterbium(III) Emission as an Internal Standard

P. Stanley May, [*] *Aravind Baride, Md Yeathad Hossan, Mary Berry*

Department of Chemistry, University of South Dakota, Vermillion, SD, 57069

[*] *Communicating author*

Abstract. A method is presented for estimating the internal quantum yield (*IQY*) of NIR-to-NIR and NIR-to-visible upconversion (UC) luminescence for Yb^{3+}-sensitized energy-transfer upconversion (ETU) phosphors. The method does not require an integrating sphere or a secondary standard, but rather uses the 1 μm emission of the Yb^{3+} sensitizer as an internal standard. The method requires the acquisition of the 1 μm emission decay curve of the UC phosphor using low pulse-energy density, an estimation of the radiative decay constant of the 1 μm emission, and emission spectra corrected for instrument response. This method is valid for UC emission spectra acquired via pulsed or continuous wave (cw) excitation. The method is demonstrated for cw excitation to obtain *IQY* for UC and downshifted luminescence for β-phase $NaYF_4$: 0.5%Tm, 25%Yb and $NaYF_4$:2%Er, 18%Yb nanocrystals (with and without a passivating $NaYF_4$ shell) over a range of excitation irradiance. The corresponding results are consistent with those obtained using integrating spheres and numerical simulations, respectively. For pulsed excitation, an additional alternative method is described which requires acquisition of the 1 μm emission decay curve at each excitation pulse-energy density for which the *IQY* is to be determined. The proposed methods should be particularly useful for samples having very low absorbance at the excitation wavelength, for which direct determination methods are impractical.

1. Introduction

In 2004, the first methods for producing solvent dispersible nanoparticles capable of upconverting near-infrared (NIR) excitation to shorter-wavelength emission were introduced.[1,2] These upconverting nanocrystals (UCNC) were based on the lanthanide-doped fluoride lattice, $NaYF_4$, co-doped with Yb^{3+} and Ln^{3+} ($Ln^{3+}= Er^{3+}$, Tm^{3+}). Since then, tremendous progress has been made in understanding and manipulating the optical properties of upconversion nanomaterials. The luminescent properties of UCNC can be tuned through particle size, phase, morphology, matrix, dopant ions, active and passive shells on the nanocrystal 'core', excitation irradiance, sensitizing organic ligands, and plasmonic nanostructures.[3-6] Moreover, UCNC are being investigated for a wide range of applications, including bioimaging, theranostics, photovoltaics, and anti-counterfeiting, all of which have been excellently reviewed.[3,7-14]

In spite of this substantial progress, it can still be difficult to compare results obtained from different studies on UCNC in a meaningful way. This is due in part to the non-linear dependence of UC behavior on excitation intensity. Often, key behavioral aspects of UC materials depend on the excitation irradiance (or pulse-energy density) used. For example, the brightness enhancement factors achieved through passive-shell addition[15,16] or metal-surface interactions[5,17] tend to diminish as excitation irradiance increases. In fact, even the optimal doping concentrations for UCNC can depend on irradiance.[18,19] Even so, the results for many UCNC studies are reported for only a single irradiance value, which complicates extrapolation to other excitation conditions.

2

Also, the quantitative results for UCNC investigations will, in general, depend on the nature of the specific UCNC sample used. Imaging sensitivity, for example, will clearly depend on the brightness of the UCNC being imaged. The benefits of shell addition will depend not only on the irradiance being employed, but also on the level of surface quenching in the core UCNC. So, the question often arises: "How do my nanocrystals compare to your nanocrystals?" The size, morphology and doping levels of UCNC are commonly reported, but there is no straightforward way to predict the photo-physical behavior of the materials based on these parameters. This is especially true in cases for which the UCNC have undergone some type of post-synthetic modification (e.g., ligand exchange, shell addition).

There is then a clear need for a set of descriptors that can be used to convey the photo-physical properties of UCNC in a useful manner. We have previously suggested that, for Yb-sensitized UCNC, the total decay constant for the 1 μm emission obtained by direct excitation into Yb^{3+} at low excitation pulse-energy density, $k_{1\mu m}^{low}$, is a useful descriptor for these materials and a powerful predictor of upconversion behavior.[15] This is because the extent of quenching of the energy reservoir for upconversion at the 1 μm level is the dominant factor in determining subsequent UC efficiency. For the specific case of hexagonal-phase $NaYF_4$: 2%Er, 18% Yb UCNC, we have published plots from which it is possible to estimate the internal quantum yield (*IQY*) of UC at a given irradiance if the value of $k_{1\mu m}^{low}$ is known.[15]

In addition to $k_{1\mu m}^{low}$, a more general and complete descriptor of UCNC luminescent behavior would be the *IQY* as a function of irradiance (or pulse-energy density). Unfortunately, such data

is relatively rare in the literature.[16,20-33]   Most reports of *IQY* for UCNC are based on direct determination using integrating spheres.   While direct-determination methods are probably the best,[30,34] they require specialized equipment and a level of expertise not readily available to most investigators in the field. Moreover, direct-measurement methods typically require the sample to have a measurable absorbance (≥ 0.03) at the excitation wavelength. Many important UC studies involve thin films or dilute dispersions with no appreciable absorbance. For example, the study of the plasmonic enhancement effects of patterned noble-metal surfaces usually involves the interaction of the surface with very thin films of the upconversion phosphors.[5,17,35,36] For bio-conjugated UCNC, or UCNC which have been otherwise surface-modified for aqueous dispersions, it can be impractical to produce stable dispersions with optical densities sufficient for integrating sphere methods. Moreover, water has significant absorbance at 980 nm, which makes it quite difficult to accurately isolate the absorbance due to UCNC.

Here, we present a method, which should be accessible to many groups working in the field, for estimating the internal quantum yield (*IQY*) of NIR-to-NIR and NIR-to-visible upconversion (UC) luminescence for Yb^{3+}-sensitized energy-transfer upconversion (ETU) phosphors. The method does not require an integrating sphere or a secondary standard, but rather uses the 1 μm emission of the Yb^{3+} sensitizer as an internal standard. The method requires the acquisition of the 1 μm emission decay curve of the UC phosphor using low pulse-energy density, an estimation of the radiative decay constant of the 1 μm emission, and emission spectra that are corrected for instrument response. It is valid for UC emission spectra acquired via pulsed or continuous wave (cw) excitation. For pulsed excitation, an additional alternative method is also

described, which requires acquisition of the 1 µm emission decay curve at each excitation pulse-energy density for which the *IQY* is to be determined.

Nanoparticles of β-NaYF$_4$: 0.5%Tm, 25%Yb with and without an added shell of NaYF$_4$ were chosen for this study because Fischer, et al have used an integrating-sphere technique to determine the internal quantum yield, *IQY*, of the 980nm-to-800nm upconversion of β-NaYF$_4$: 0.5%Tm, 25%Yb@ NaYF$_4$ using cw excitation over a range of excitation irradiance.[37] Therefore, the results obtained with our method can be directly compared to published results for an integrating sphere method. In addition, samples of β-NaYF$_4$:2%Er, 18%Yb core and β-NaYF$_4$:2%Er, 18%Yb@ NaYF$_4$ core-shell nanoparticles were selected for study, because the experimentally-determined *IQY* can be compared to the simulated results reported by Hossan, et al.[15] The corresponding results obtained from the proposed method are consistent with those obtained using integrating spheres and numerical simulations, respectively. The proposed method should be particularly useful for samples having very low absorbance at the excitation wavelength, for which direct determination methods are impractical. It might also find utility as a consistency check for direct *IQY* measurements.

2. Background

The measured luminescence intensity, *I,* in photons/s, for a phosphor under continuous photoexcitation is given by

$$I = F \cdot IQY \cdot P_0 \cdot \left(1 - 10^{-\varepsilon bc}\right) \qquad (1)$$

where F is the fraction of emitted photons detected by the measurement system; IQY is the internal quantum yield of the emitter, defined as $IQY = \dfrac{\text{photons emitted}}{\text{photons absorbed}}$; P_0, is the incident intensity of the excitation beam (photons/s), ε is the molar extinction coefficient of the phosphor at the excitation wavelength ($M^{-1}cm^{-1}$), b is the path length of the light through the sample (cm), and c is the molar concentration of the phosphor. Equation 1 assumes that absorbance of the excitation light by any species other than the phosphor is negligible and that there is no self-absorbance of emitted light. Equation 1 is also suitable for describing pulsed excitation, except that I becomes the total photons emitted per pulse, and P_0 becomes the total number of excitation photons per pulse.

Solving Equation 1 for IQY yields

$$IQY = C \cdot \frac{I}{P_0} \qquad (2)$$

where $C = \dfrac{1}{F \cdot \left(1 - 10^{-\varepsilon bc}\right)}$ (no units). The value of C for a given sample under a fixed set of experimental conditions (e.g., excitation and collection geometry, slit widths) will be constant. In the absence of non-linear processes, I increases linearly with P_0, such that $\dfrac{I}{P_0}$ is constant and IQY is independent of the excitation intensity. For UC emission, I will generally increase more rapidly than P_0, such that the internal quantum yield, IQY, will depend on P_0. (Note: To be precise, the IQY of UC phosphors depends on the excitation flux (photons/s/cm^2), not the excitation intensity (photons/s). However, because we have specified a fixed experimental

6

geometry, including the excitation beam geometry, the excitation flux will be directly proportional to P_0.) The key point here is that, if the value of C is known, then IQY for the sample may be calculated from the measured emission spectrum and excitation intensity, regardless of the order of the excitation process.

The intrinsic quantum yield, QY_{int}, of luminescence from a given emitting state is the fraction of phosphors that relax from that state via emission of a photon. The relative QY_{int} for a given emitting state in the presence and absence of quenchers is given by[38]

$$\frac{QY_{int}}{QY_{int}^{0}} = k_{tot}^{0} \int_{0}^{\infty} \frac{I(t)}{I(0)} dt \qquad (3)$$

where QY_{int}^{0} is the intrinsic quantum yield in the absence of quenchers; k_{tot}^{0} is the total relaxation rate constant for the emitter whose intrinsic quantum yield is QY_{int}^{0}; and $\int_{0}^{\infty} \frac{I(t)}{I(0)} dt$ is the integrated decay curve of the luminescence of the 'quenched' emitter following pulsed excitation into the emitting state, divided by the intensity immediately following the pulse, $I(0)$. If the emission decay curve conforms to a single-exponential function, then $\int_{0}^{\infty} \frac{I(t)}{I(0)} dt = \int_{0}^{\infty} e^{-k_{tot}t} dt = \frac{1}{k_{tot}}$, where k_{tot} is the total relaxation rate constant for the emitter whose intrinsic quantum yield is QY_{int}. Even in cases for which the luminescence decay curves are not simple exponentials, it is useful to define an effective k_{tot}, where $k_{tot} = \left[\int_{0}^{\infty} \frac{I(t)}{I(0)} dt \right]^{-1}$.

In fact, Equation 3 is valid for comparing relative QY_{int} values for any two otherwise-identical species undergoing different levels of quenching, regardless of the quenching mechanisms (e.g., energy transfer, multiphonon relaxation). For the special case in which QY_{int}^0 is unity, the value of k_{tot}^0 must equal the radiative relaxation rate constant, k_{rad}, for the emitting state, and Equation 3 becomes

$$QY_{int} = k_{rad} \int_0^\infty \frac{I(t)}{I(0)} dt \qquad (4)$$

For direct excitation into the emitting state, the intrinsic and internal quantum yields are the same (i.e., $QY_{int} = IQY$), and Equation 4 becomes,

$$IQY = k_{rad} \int_0^\infty \frac{I(t)}{I(0)} dt = \frac{k_{rad}}{k_{tot}} \qquad (5)$$

where $k_{tot} = \left[\int_0^\infty \frac{I(t)}{I(0)} dt \right]^{-1}$. This definition for an effective k_{tot} has the advantage of explicitly including cases, commonly encountered in nanomaterials, for which the luminescence decay curves are not simple exponentials. Thus, IQY can be calculated from measured luminescence decay curves and a reliable estimate of k_{rad}.

The methods described herein use Equation 5 to estimate the internal quantum yield for the 1 μm emission, IQY (1μm), of Yb^{3+} (or Yb^{3+} and Er^{3+}) in Yb^{3+}-sensitized upconversion materials. The luminescence spectrum of the 1 μm band is then acquired under conditions for which IQY (1μm)

matches the value determined using Equation 5. The value of C in Equation 2 is then determined using the integrated intensity of the 1 μm luminescence band, $I(1\mu m)$, the measured value of excitation power (or energy), P_0, and the estimated IQY (1μm).

In general, IQY (1μm) will depend on excitation irradiance (cw excitation) or pulse-energy density (pulsed excitation), because UC luminescence comes at the expense of 1 μm emission. It is important to ensure, therefore, that the IQY (1μm) corresponding to the emission spectrum used in Equation 2 to determine C matches the IQY (1μm) value determined from Equation 5 using pulsed excitation. If the emission spectrum is to be measured using cw excitation, the only straightforward way to ensure this condition is to acquire the 1μm decay curve (pulsed) and emission spectrum (cw) in the limit of low excitation 'intensity', for which little or no UC emission is observed. In this limit, IQY (1μm) is independent of excitation intensity and will have the same value for pulsed and cw excitation.

3. Methodology

Two methods for determining IQY for UC luminescence are described below. The first method is more general, in that it is applicable to estimating quantum efficiencies under either cw or pulsed excitation. The second method is an alternative method for use only with pulsed excitation. In all subsequent discussion, we define 'corrected' spectra as being corrected for instrument response, representing $\partial photons/\partial\lambda$ vs λ.

For the methods outlined below, it is not necessary to know the excitation irradiance (or energy density for pulsed excitation) in order to determine *IQY* from the emission spectra. However, quantum yield measurements for UC systems are of little or no value unless they can be associated with a given excitation irradiance/energy density. The cross-sectional profile of the laser beam at the sample should always be measured in order to convert the power or pulse energy to irradiance or pulse-energy density.

Method 1. Determining IQY for Upconversion Emission under Continuous Wave (cw) or Pulsed Excitation

In the regime of low excitation density, in which UC is insignificant, the internal quantum yield of the 1 μm emission, *IQY* (1μm), will be largely independent of excitation 'intensity', and $\dfrac{I}{P_0}$ will be constant. (See Equation 2) Therefore, if the value of *IQY*(1μm) in the low power regime is known, the value of *C* in Equation 2 can be determined for a specific experimental geometry from the low-power 1 μm emission spectrum and the measured excitation power or pulse energy used to acquire the spectrum.

Here, we use the measured 1μm decay curve and the estimated radiative rate constant, k_{rad}, for the 1 μm emission to estimate *IQY* (1μm) in the low power regime, henceforth referred to as *IQY*(1μm; low), according to Equation 5. A low excitation pulse-energy density, exciting directly into the Yb^{3+}: $^2F_{7/2} \rightarrow ^2F_{5/2}$ transition, is used to acquire the decay curve for the 1 μm emission for the sample of interest. The decay curve can then be used to determine

$$\int_0^\infty \frac{I\left(t\right)}{I\left(0\right)}dt = \left(k_{1\mu m}^{low}\right)^{-1}$$, as described in the Background section, where $k_{1\mu m}^{low}$ represents the effective

total decay constant, k_{tot}, for the 1 μm emission at low pulse-energy density.

Because the Yb^{3+}: $^2F_{7/2} \rightarrow ^2F_{5/2}$ transition is not hypersensitive, k_{rad} does not vary dramatically

from compound to compound, and is generally on the order of 500 s^{-1} for fluoride lattices.

Krupke reports k_{rad} values for Yb^{3+} across a series of crystalline hosts[39] and it can be shown that

k_{rad} varies predictably as a function of the refractive index, n, of the host, indicating that the

variation is due mainly to changes in the electric field experienced by the Yb^{3+} ion. (See SI) The

trend in Krupke's data would predict $k_{rad}= 498$ s^{-1} for Yb^{3+} in $NaYF_4$ ($n= 1.497$). (See SI) The

k_{rad} value for Yb^{3+} in any crystal host can therefore be reasonably approximated from the

refractive index of the host. It is also possible to estimate k_{rad} from absorbance spectra.[40] For

Yb/Er co-doped systems, Er^{3+} will also contribute to the 1 μm emission. For β-$NaYF_4$: 2%Er,

18%Yb at room temperature, we have used our previous rate-equations analysis[15] to estimate k_{rad}

$= 506$ s^{-1}, which includes the contribution from Er^{3+} emission.

For nanoparticle emitters, k_{rad} can be affected by the refractive index of the solvent, and this

effect can be quantitatively determined.[41] The effect is notable only when the refractive indexes

of the nanoparticle and dispersal medium differ significantly. The k_{rad} for dopants of β-$NaYF_4$

UCNC dispersed in toluene should be virtually identical to that in the bulk.

The value of $\dfrac{I}{P_0}$ (low-power) is determined from the integrated intensity, I, of a corrected 1 µm

emission spectrum obtained by exciting with a low pulse-energy density or irradiance (for cw),

P_0. The value of the geometric constant, C, can then be determined according to

$$C = IQY\left(1\mu m;\ low\right) \cdot \frac{P_0}{I(1\mu m)} \quad (low\ irradiance) \qquad (6)$$

The units used for P_0 are unimportant, as long as the same units are used for all spectra.

The UC spectra are then acquired over the excitation power/energy density range for which IQY

values are desired, using exactly the same experimental parameters and geometry as used for the

determination of C. The excitation power/energy density must be varied in such a way so as to

not change the spatial profile (e.g., focus) of the beam. Ideally, the sample is not disturbed

following acquisition of the low-power spectrum, and all subsequent spectra are measured in one

experimental session to minimize the possibility of any experimental variation. We also note

that, while it is not necessary to include the 1 µm region in these higher-power emission scans in

order to determine the IQY for the UC transitions, the 1 µm emission serves as a useful internal

check on the accuracy and consistency of the measurements, as will be demonstrated later.

The instrument-response corrected UC spectra, representing relative $\partial photons/\partial\lambda$ vs λ, are then

multiplied by $\dfrac{C}{P_0}$, where P_0 is the excitation intensity used to acquire each spectrum. The

resulting spectral representations correspond to $\partial(IQY)/\partial\lambda$ vs. λ. At this point, the IQY of each

luminescence band is equal to its integrated area in the spectrum.

12

Method 2. Alternate Method for Determining *IQY* for Upconversion Emission under Pulsed Excitation.

For pulsed excitation, there is an additional option to calculate a separate *C* for each pulse-energy density for which *IQY* values are desired. The advantage to this alternate method is that *IQY* values can be determined from a single emission spectrum and a single decay curve measurement made at the same pulse energy and pulse-energy density. Using this method, it is unnecessary to maintain otherwise identical experimental conditions when comparing data taken under different excitation energy densities, because an independent *C* value is determined for each spectrum. The *IQY* for the 1 μm luminescence corresponding to each of those pulse-energy densities can then be determined separately using Equation 5. The value of *C* is then determined separately for each spectrum according to $C = IQY(1\mu m) \cdot \dfrac{P_0}{I(1\mu m)}$. From this point, the *IQY* for the UC and 1 μm luminescence are determined as described for Method 1.

The major disadvantage to the alternate method is that the 1 μm decay curve becomes increasingly non-exponential in shape with increasing pulse-energy density, such that the determination of $\displaystyle\int_0^\infty \frac{I(t)}{I(0)}dt = \frac{1}{k_{1\mu m}}$ becomes less reliable. This is due mainly to the potential contribution of scatter to the decay signal at t=0, making it difficult to accurately determine the value of $I(0)$.

4. Experimental

4.1 Synthesis of β-NaYF$_4$:Ln, Yb core nanocrystals

Nanocrystal samples of β-NaYF$_4$:0.5%Tm, 25%Yb and β-NaYF$_4$:2%Er, 18%Yb were synthesized as previously described,[15] based on the 'heat up' method developed by Zhang, et al.[42,43] Phase purity was confirmed by powder XRD (Rigaku).

4.2 Addition of β-NaYF$_4$ shell to β-NaYF$_4$:Ln, Yb core nanocrystals

Un-doped NaYF$_4$ shell material was added to the β-NaYF$_4$: 0.5%Tm, 25%Yb and β-NaYF$_4$: 2%Er, 18%Yb core nanocrystals as previously described,[15] based on a procedure developed by Johnson, et al.[44] In brief, small (8-10 nm) α-phase particles of NaYF$_4$ are added to a dispersion of the β-NaYF$_4$:Ln, Yb core nanocrystals in solvent composed of oleic acid and octadecene. The resulting mixture is then heated to 310°C under constant stirring.   The completion of the shell addition is determined using a system that monitors the upconversion luminescence of the reaction mixture.[45] Phase purity is confirmed by powder XRD (Rigaku).

4.3 Electron Microscopy

The morphology and size distribution of all core and core-shell nanocrystal samples were determined by SEM (Zeiss) and / or TEM (FEI). Nanocrystal samples were dispersed in toluene

and then dropped onto either a copper grid, for TEM measurements, or a silicon substrate, for SEM analysis.

4.4 Spectroscopic measurements

All luminescence measurements were made using a 90° excitation-collection geometry on nanocrystals dispersed in toluene and placed in a 4 mm × 4 mm cuvette (Starna, SOG). The dispersion concentrations were ≤12 mg/mL for all samples. The dispersions were of high optical quality, showing no notable coloration or turbidity (see Fig. 1). No detectable absorbance due to water in the 1 μm region was observed. The absorbance due to Yb^{3+} at the excitation wavelengths used was ≤0.004, far below that normally required for integrating sphere methods. Sample temperature was maintained at 25°C for all measurements. Time-dependent decay curves of 1 μm luminescence were acquired using pulsed 950 nm excitation (20Hz; 5 ns FWHM) from an optical parametric oscillator, OPO (OPOTEK, Opolette HE 355 LD). The laser beam was left unfocused (4 mm beam diameter) and pulse-energy densities were held below 15 mJ/cm^2/pulse to avoid interference from non-linear processes. For acquisition of steady-state luminescence spectra, excitation light was provided by a nominal 940 nm laser diode (Sheaumann Laser, M9-940-0300-D5P) on a temperature-controlled mount (Thorlabs TCLDM9). The actual measured output wavelength of the diode used was 936 nm. The diode was operated at a constant power output in order to maintain a stable beam profile, and optical density filters (Bausch & Lomb) mounted in a rigidly-fixed holder were used to change the irradiance on the sample dispersions. Optical density filters were determined to reproducibly attenuate the irradiance without effecting the beam profile or position at the sample. The cross-sectional intensity distribution of the diode

laser beam was characterized using a digital camera (ThorLabs, DCC3240N) placed at the sample position. (See Fig. 1) The beam exhibited a Gaussian intensity distribution; the power density values reported here were calculated based on defining the spatial boundaries of the beam at the 2σ values of the intensity distribution. For each cw spectrum, laser power was measured both immediately in front and immediately behind the sample cuvette (Thorlabs, S120C (sensor); PM100D (meter)). For both pulsed and cw measurements, sample luminescence was focused into a flat-field spectrograph (Horiba, iHR320) equipped with a UV-NIR sensitive (185-1010 nm) photomultiplier tube, PMT (Hamamatsu, R2658P) on the axial detector port, and a NIR-sensitive (950-1700 nm) PMT (Hamamatsu, H10330A-75) on the lateral detector port. The PMT signal was pre-amplified (SRS, SR445A) prior to input into to a time-resolved photon-counting system (SRS, SR430 Multichannel Scalar).
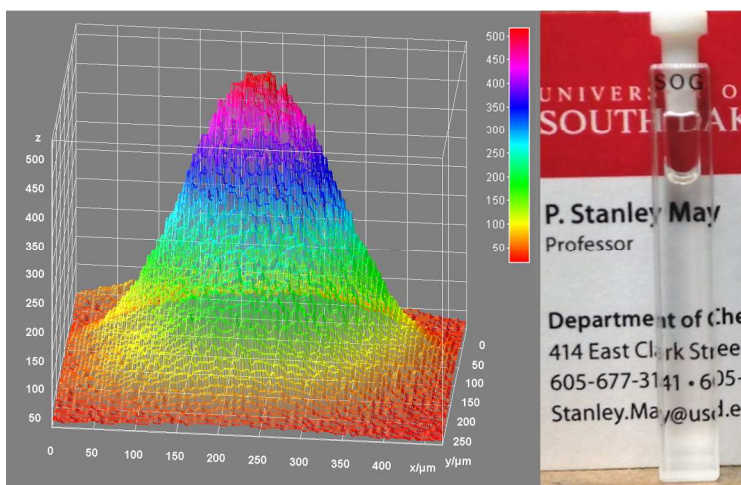

Figure 1. (Left) Cross-sectional intensity profile of excitation laser beam used to acquire the luminescence spectra in this study. The horizontal spatial scales are in units of μm. (Right) Photo of 4 mm × 4 mm cuvette containing the dispersion of β-NaYF$_4$: 2%Er, 18%Yb@NaYF$_4$ core-shell nanocrystals in toluene used in this study to acquire luminescence spectra which were subsequently analyzed to determine internal quantum yields (IQY).

For comparison purposes, it is convenient to convert the excitation irradiance values at the 936 nm wavelength used in this study for cw measurements to the corresponding irradiance values at the Yb^{3+} absorbance maximum of 976 nm which would be required to achieve an equivalent Yb^{3+} excitation rate. This was accomplished by scaling to the relative Yb^{3+} absorbance at 976 nm and 936 nm. Absorbance spectra of the nanoparticle samples were obtained from concentrated dispersions of the nanocrystals in CCl_4 made specifically for this purpose. (See Supporting Information) Carbon tetrachloride was used as a solvent because it is completely transparent in the NIR.

5. Results and Discussion

5.1 Internal quantum yield (IQY) of luminescence in β-NaYF$_4$: 0.5%Tm, 25%Yb@ NaYF$_4$ core-shell and β-NaYF$_4$: 0.5%Tm, 25%Yb core nanoparticles under continuous wave (cw) NIR excitation

5.1.1 Nanocrystal Size and Morphology

Figure 2 shows SEM images of the β-NaYF$_4$: 0.5%Tm, 25%Yb core and β-NaYF$_4$: 0.5%Tm, 25%Yb@NaYF$_4$ core-shell nanocrystals. The core nanocrystals are hexagonal prisms with an aspect ratio close to 1; the average edge-to-edge width across the hexagonal face is 71.8±2.5 nm and the length along the c-axis is 68.4±1.3 nm. Addition of the NaYF$_4$ shell to the core nanocrystals results in an increase in crystal size (width × length= 89.6 + 2.5 nm × 79.6 + 2.4 nm), more pronounced hexagonal faceting, and a slight reduction in the aspect ratio. The shell thickness for the core-shell nanocrystals is 5.6 nm on the axial (hexagonal) faces and 8.9 nm on the orthoaxial faces. The dimensions of the crystals are summarized in Table 1.

We note that, during the addition of the inert $NaYF_4$ shell, small nanocrystals of undoped β-$NaYF_4$ are produced, some of which can be observed in Figure 2 (lower image). These arise because Ostwald ripening of the sacrificial α-$NaYF_4$ nanocrystals results in a small fraction growing past the size threshold whereby they spontaneously convert to the β phase.[46] We typically observe this phenomenon only when adding a thick shell, which provides a reaction time long enough for sufficient ripening of the α-$NaYF_4$ nanocrystals for the phase transition to occur. We have confirmed through energy-dispersive X-ray spectroscopy (EDS) that these small crystals contain no Yb, and are, therefore, optically silent in our experiments.
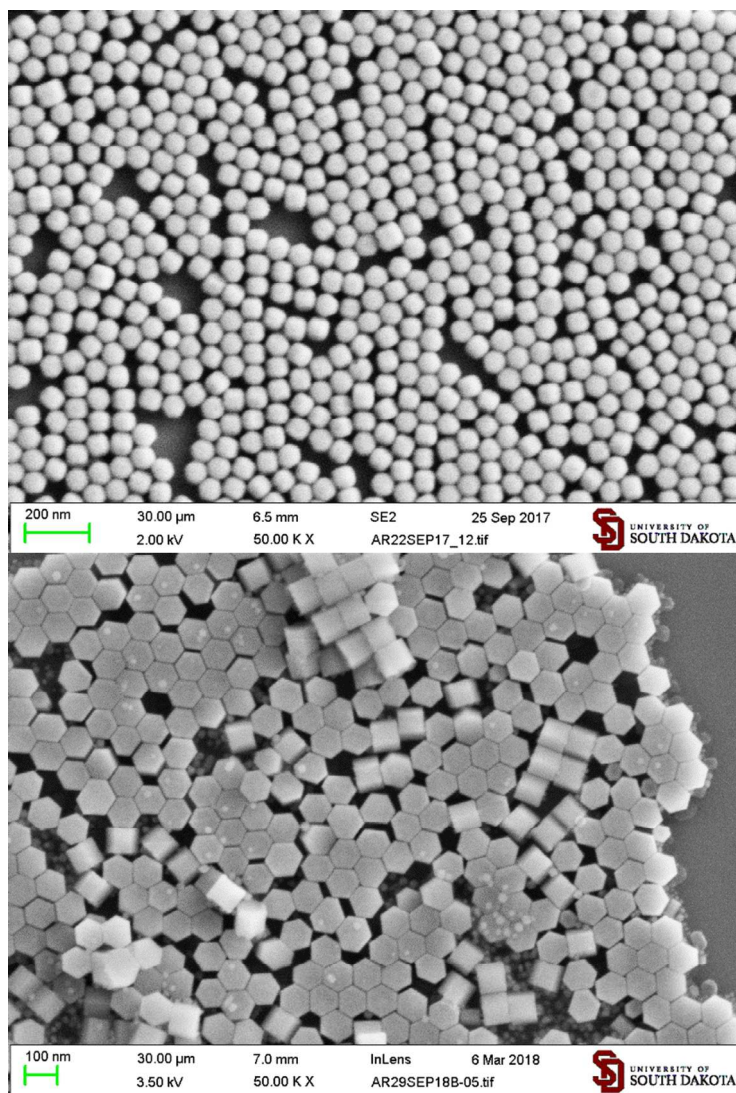
Figure 2. SEM images of β-NaYF$_4$:0.5%Tm, 25%Yb core (upper panel) and β-NaYF$_4$:0.5%Tm, 25%Yb@NaYF$_4$ core-shell (lower panel) nanocrystals. The dimensions of the crystals are summarized in Table 1.

Table 1. Dimensions of β-NaYF$_4$: 0.5%Tm, 25%Yb core and β-NaYF$_4$: 0.5%Tm, 25%Yb@NaYF$_4$ core-shell nanocrystals

Sample	Width (nm)	Length (nm)	Aspect ratio length/width	Ortho-face shell (nm)	Axial-face shell (nm)
β-NaYF$_4$: 0.5%Tm, 25%Yb	71.8±2.5	68.4±1.3	0.95	---	---
β-NaYF$_4$: 0.5%Tm, 25%Yb@NaYF$_4$	89.6±2.5	79.6±2.4	0.89	8.9	5.6

5.1.2 Upconversion and downshifted luminescence spectrum for β-NaYF$_4$: 0.5%Tm, 25%Yb@NaYF$_4$ core-shell nanocrystals

Figure 3 shows the luminescence spectrum, expressed as relative δphotons/δλ vs λ, of β-NaYF$_4$: 0.5%Tm, 25%Yb@NaYF$_4$ core-shell nanocrystals obtained using 936 nm excitation at 534 W/cm^2, the highest excitation irradiance used in this study. These excitation conditions provide an excitation rate equivalent to 76 W/cm^2 at the Yb^{3+} absorbance maximum near 976 nm. The downshifted emission at 1 μm is from Yb^{3+}; all other bands are assigned to Tm^{3+}. Note that the NIR-to-NIR upconversion at 800 nm, corresponding to the $^3H_4 \rightarrow ^3H_6$ transition of Tm^{3+} is much more intense than the higher-order NIR-to-visible Tm^{3+} emission from the $^1D_2$ and $^1G_4$ levels, and is of the same order of magnitude of intensity as the Yb^{3+}: $^2F_{5/2} \rightarrow ^2F_{7/2}$ emission at 1 μm.
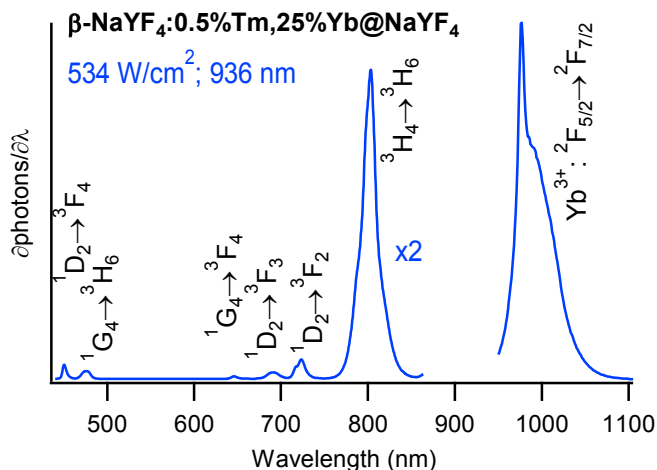
Figure 3. Luminescence spectrum of β-NaYF$_4$: 0.5%Tm, 25%Yb@NaYF$_4$ core-shell nanocrystals dispersed in toluene using 936 nm excitation at 534 W/cm^2, corrected to represent relative δphotons/δλ vs λ. The excitation rate is equivalent to 76 W/cm^2 at the Yb^{3+} absorbance maximum near 976 nm.

5.1.3 Determination of IQY(1µm; low) for β-NaYF$_4$: 0.5%Tm, 25%Yb@NaYF$_4$ core-shell and β-NaYF$_4$: 0.5%Tm, 25%Yb core nanocrystals

Figure 4 shows the decay curves of Yb^{3+} emission monitored at 976 nm following pulsed excitation at 950 nm for the core and core-shell samples dispersed in toluene. The pulse-energy density used to acquire the decay curves was reduced until little or no UC emission was detectable in order to ensure minimal contribution from non-linear processes to the curve shape. For the core-shell sample, the curve fits well to an exponential function, such that

$$\int_0^\infty \frac{I\,(t)}{I\,(0)}dt = \int_0^\infty e^{-k_{tot}t}dt = \left(k_{1\mu m}^{low}\right)^{-1} = (1.237\pm0.003)\times10^{-3} \text{ s (See section 2), corresponding to } k_{1\mu m}^{low}$$

=808±2 s^{-1}. For the core sample, the curve shape deviates significantly from an exponential

function and $\int_0^\infty \dfrac{I(t)}{I(0)}dt = \left(k_{1\mu m}^{low}\right)^{-1} = (3.006\pm0.040)\times10^{-4}$ s, corresponding to $k_{1\mu m}^{low} = 3327\pm44$ s^{-1}.

The value of the radiative rate constant, k_{rad}, was estimated to be $k_{rad} = 525$ s^{-1},[15] so that, according to Equation 5, the quantum yield of the Yb^{3+} emission in the 'low power' region is

$$IQY(1\mu m; low) = \frac{k_{rad}}{k_{1\mu m}^{low}} = \frac{525 s^{-1}}{808 s^{-1}} = 0.650 \qquad \text{for} \qquad \text{the} \qquad \text{core-shell} \qquad \text{sample} \qquad \text{and}$$

$$IQY(1\mu m; low) = \frac{k_{rad}}{k_{1\mu m}^{low}} = \frac{525 s^{-1}}{3327 s^{-1}} = 0.158 \text{ for the core sample. These results are summarized in}$$
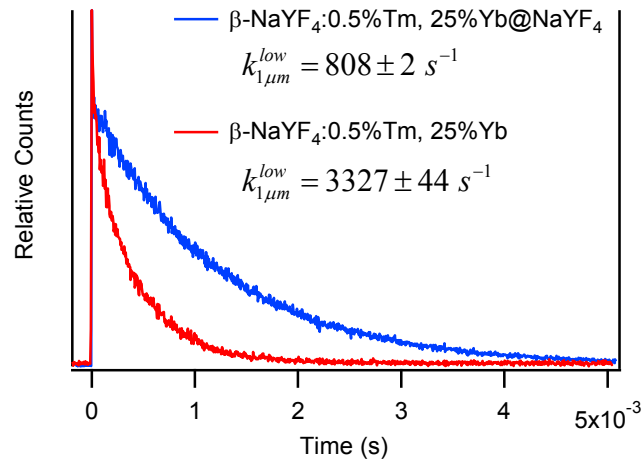
Table 2.

Figure 4. Time dependence of 976 nm emission of Yb^{3+} following pulsed excitation at 950 nm for β-NaYF$_4$: 0.5%Tm, 25%Yb@ NaYF$_4$ core-shell and β-NaYF$_4$: 0.5%Tm, 25%Yb core nanocrystals. The pulse-energy density used to acquire the decay curves was reduced until little or no UC emission was detectable to ensure minimal contribution from non-linear processes.

Table 2. Inputs used to calculate the internal quantum yields for Yb^{3+} emission in β-NaYF$_4$: 0.5%Tm, 25%Yb@ NaYF$_4$ core-shell and β-NaYF$_4$: 0.5%Tm, 25%Yb core nanocrystals in the limit of low excitation irradiance according to Equation 5.

Sample	$k_{1\mu m}^{low}$ (s^{-1})	$k_{rad}(s^{-1})$	$IQY\left(1\mu m;low\right)$
Core-shell	808	525	0.650
Core	3327	525	0.158

5.1.4 Internal quantum yield, IQY, of β-NaYF$_4$: 0.5%Tm, 25%Yb@ NaYF$_4$ core-shell and β-NaYF$_4$: 0.5%Tm, 25%Yb core nanocrystals as a function of excitation irradiance

Corrected luminescence spectra (δphotons/δλ vs λ) of β-NaYF$_4$: 0.5%Tm, 25%Yb@ NaYF$_4$ core-shell and β-NaYF$_4$: 0.5%Tm, 25%Yb core nanocrystals dispersed in toluene were measured for a series of excitation power densities under otherwise identical experimental conditions. Each series includes a spectrum of the 1 μm emission band acquired using excitation irradiance reduced to the point at which little or no upconversion could be observed.

Equation 6 was then applied using the spectrum acquired at the lowest excitation irradiance in the series (for which little or no upconversion was observed) to determine the geometric constant, C. In this case, $I\left(1\mu m\right)$ is the integrated intensity of the 1 μm luminescence in the low-irradiance spectrum, P_0 is the excitation irradiance used to acquire that spectrum, and the value of $IQY\left(1\mu m;low\right)$ is given in Table 2.

The instrument-response corrected δphotons/δλ values of each spectrum in the series were then multiplied by $\dfrac{C}{P_0}$, where P_0 is the excitation irradiance used to acquire each spectrum. At this

point, the spectral representations correspond to $\partial(IQY)/\partial\lambda$ vs. λ, and integrated areas correspond to internal quantum yield, *IQY*, of the emission within the spectral range of integration (See Equation 2). The resulting $\partial(IQY)/\partial\lambda$ vs. λ spectra for the core-shell sample are shown for three excitation-irradiance values in Figure 5. The *IQY* for Tm^{3+} upconversion emission shows the expected increase with increasing irradiance, whereas the *IQY* for the Yb^{3+} 1 μm emission notably decreases with increasing excitation irradiance due to depletion of $Yb^{3+}(^{2}F_{5/2})$ excited state by the upconversion process.
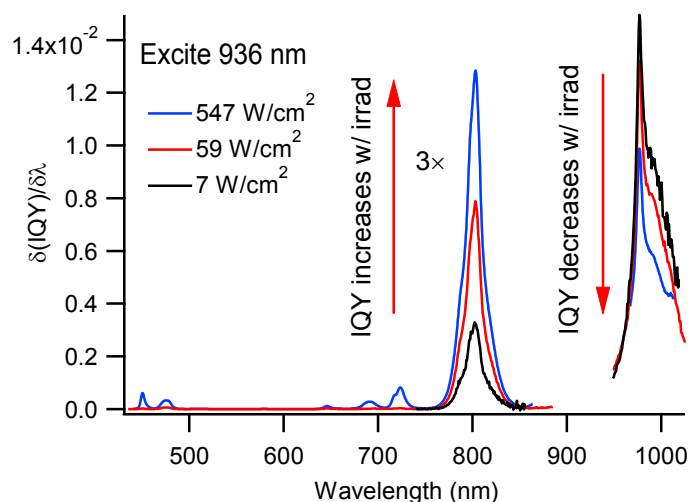

Figure 5. $\partial(IQY)/\partial\lambda$ vs. λ spectra of β-NaYF$_4$: 0.5%Tm, 25%Yb@NaYF$_4$ core-shell nanocrystals dispersed in toluene using 936 nm excitation at irradiances of 547, 59, and 7 W/cm^2. These irradiance values generate excitation rates equivalent to 78, 8.5, and 1.0 W/cm^2 at 976 nm. The $\partial(IQY)/\partial\lambda$ axis has quantitative meaning, in that the area under each emission band equals the corresponding internal quantum yield, *IQY*, of that band.

Figure 6 compares the *IQY* results obtained for the core and core-shell samples. Although the spectral data were acquired using 936 nm excitation in order to obtain the major portion of the Yb^{3+}: $^{2}F_{5/2} \rightarrow {}^{2}F_{7/2}$ emission spectrum, the irradiance scale in Figure 6 has been corrected to the irradiance required to produce an equivalent excitation rate near the Yb^{3+} absorbance maximum of 976 nm, which is the most common excitation wavelength used for Yb-sensitized upconversion systems. The upper panel of Figure 6 shows the *IQY* for the Tm^{3+}: $^{3}H_{4} \rightarrow {}^{3}H_{6}$ transition, centered at 800 nm, over the range of excitation irradiance measured. The middle panel of Figure 6 shows *IQY* vs. excitation irradiance for the Yb^{3+}: $^{2}F_{5/2} \rightarrow {}^{2}F_{7/2}$ transition at 1 μm. Also included in the middle panel are the values of *IQY*(1 μm)+2×*IQY*(800nm), representing the *IQY* of each significant emission multiplied by the number of photons required to reach the emitting state. The lower panel of Figure 6 shows the Enhancement factor, *EF*, resulting from shell addition, where $EF = \dfrac{IQY(core-shell)}{IQY(core)}$.

 The relatively high *IQY* of the 800 nm NIR-to-NIR upconversion for the core-shell sample is striking, reaching 8% at the modest excitation irradiance of 20 W/cm^{2}. Extrapolation of the trend in Figure 6 would lead one to estimate that the *IQY* of 800 nm upconversion will plateau in the range of 10%. The *IQY* of the 800 nm emission for the core sample is notably lower than that of the core-shell, as expected. The Enhancement Factor, *EF*, of the 800 nm upconversion resulting from shell addition (Fig. 6, bottom panel) is greatest at low irradiance values, consistent with previous observations that shell addition is most beneficial for low-irradiance applications.[15,37]

The *IQY* vs irradiance plots for the 1 μm emission of Yb^{3+} in the middle panel of Figure 6 shows that the increased *IQY* of the 800 nm emission comes at the expense of the $Yb^{3+}(^2F_{5/2})$ excited-state population, with the *IQY* of the Yb^{3+} 1 μm emission dropping as the *IQY* of the Tm^{3+} 800 nm emission rises.   It is interesting to note that the *EF* for the 1 μm emission (Figure 6, lower panel) is relatively insensitive to irradiance.

It is interesting to note that the 800 nm and 1 μm *IQY* behavior in Figure 6 show very good internal consistency for the core and the core-shell sample. To illustrate this, the middle panel of Figure 6 includes plots of the sum of the *IQY* for the 1 μm emission plus 2×*IQY* for the 800 nm emission. These plots are relatively constant with excitation irradiance, showing that the loss in *IQY*(1 μm) is almost quantitatively accounted for by the increase in *IQY*(800 nm), taking into account that 800 nm emission occurs via a two-photon process.
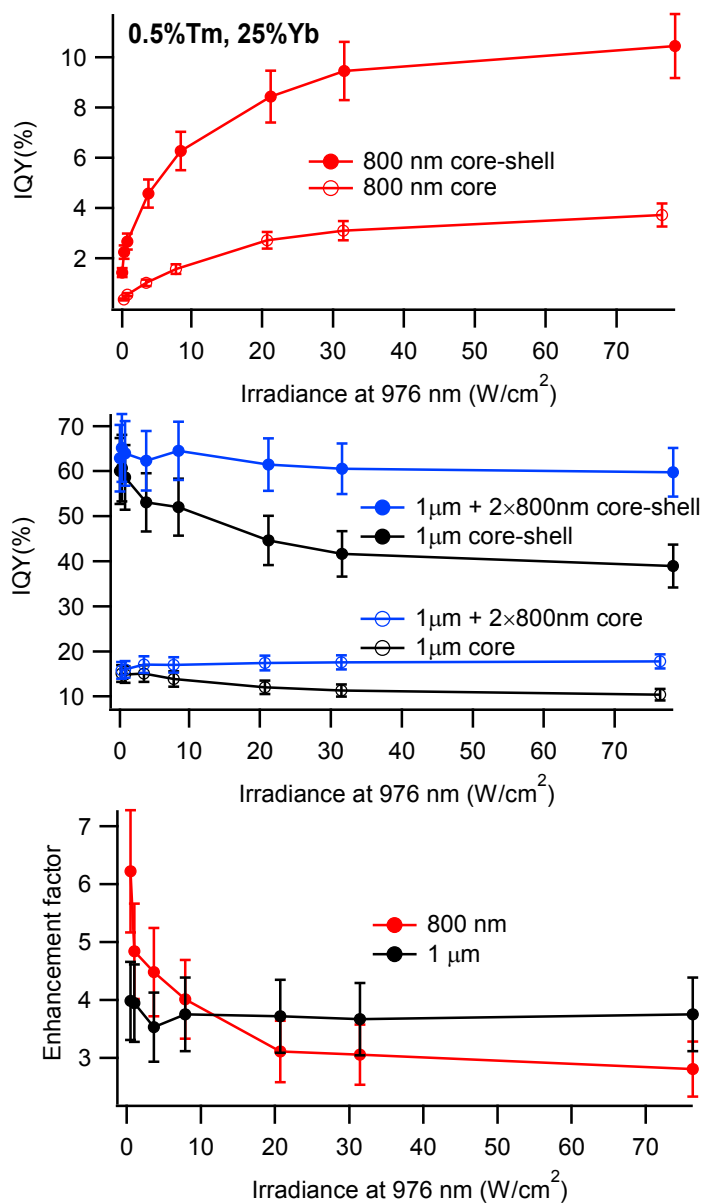
Figure 6. (Upper panel) *IQY* for the Tm^{3+}: $^3H_4\rightarrow^3H_6$ transition at 800 nm vs excitation

irradiance at 976 nm for β-NaYF$_4$: 0.5%Tm, 25%Yb@NaYF$_4$ core-shell and β-NaYF$_4$: 0.5%Tm,

25%Yb core nanocrystals. (Middle panel) *IQY* vs. excitation irradiance at 976 nm for the Yb^{3+}:

$^2F_{5/2}\rightarrow^2F_{7/2}$ emission at 1 μm for the core-shell and core samples. Also shown are plots of the

sum of *IQY* for the 1 μm emission plus 2×*IQY* for the 800 nm emission. (Lower panel)

Enhancement factors, *EF*, vs irradiance for the 1 μm and 800 nm emission, where

$$EF = \frac{IQY(core-shell)}{IQY(core)}.$$ The IQY error bars are the most probable error based on assigning a 5% uncertainty value in each rate constant and integrated intensity value used to calculate IQY. The resulting errors are 12% of the IQY value. The Enhancement factor error bars are the most probable error based on the 12% probable error in the core and core-shell IQY values.

As mentioned previously, Fischer et al. have reported the *IQY* for the Tm^{3+}: $^3H_4 \rightarrow ^3H_6$ upconversion emission at 800 nm in β-NaYF$_4$: 0.5%Tm, 25%Yb @NaYF$_4$ core-shell nanocrystals as a function of irradiance.[37] In their study, they coated nearly spherical 23.7 ± 1.2 nm diameter nanocrystals of β-NaYF$_4$: 0.5%Tm, 25%Yb with an 8.1 nm-thick isotropic shell of β-NaYF$_4$. Fortunately, they also provide the rate constant for the decay of the 1 μm emission of Yb^{3+}, and, although they do not say so explicitly, the highly exponential nature of the time profile of the 1 μm emission would indicate the use of a low excitation pulse-energy density to obtain the data. This allows us to compare the relative effects of surface or defect quenching in our samples vs theirs by comparing the values of $k_{1\mu}^{low}$.

Figure 7 compares our results for the IQY of the 800 nm upconversion emission in β-NaYF$_4$: 0.5%Tm, 25%Yb core and β-NaYF$_4$: 0.5%Tm, 25%Yb @NaYF$_4$ core-shell nanocrystals to those of Fischer.[37] The data sets are all quite consistent with each other. The *IQY* values measured for our core-shell nanocrystals are understandably higher than those of Fischer, given the significantly increased surface quenching in Fischer's sample, as indicated by the higher $k_{1\mu}^{low}$

value (1112 s^{-1} vs 808 s^{-1}) as shown in Figure 7.   Conversely, the IQY values measured for our core nanocrystals are notably lower than the Fischer sample, as would be expected from the relative $k_{1\mu}^{low}$ values (1112 s^{-1} vs 3327 s^{-1}) given in Figure 7.
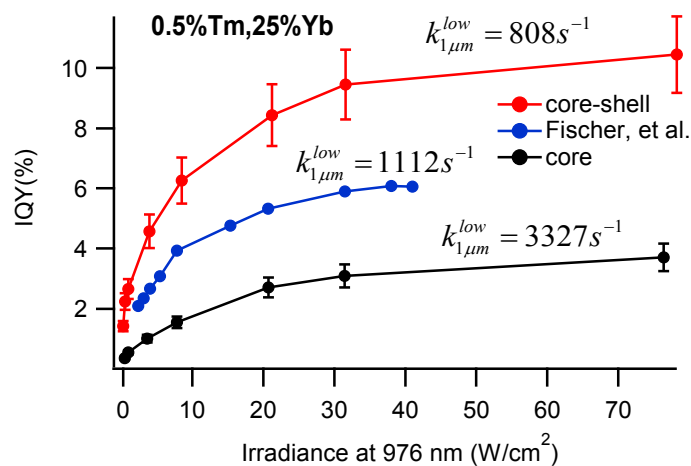

Figure 7. Comparison of *IQY* measurements of the present study to those of Fischer, et al.[37] for the 800 nm upconversion emission corresponding to the Tm^{3+}: $^3H_4 \rightarrow ^3H_6$ transition in β-NaYF$_4$:0.5%Tm, 25%Yb@NaYF$_4$ core-shell and β-NaYF$_4$:0.5%Tm, 25%Yb@ core nanocrystals. The total decay rate constant for the Yb^{3+} 1 μm emission measured using low excitation pulse-energy density, $k_{1\mu}^{low}$, is given for all samples. The error bars are the most probable error based on assigning a 5% uncertainty value in each rate constant and integrated intensity value used to calculate IQY. The resulting errors are 12% of the IQY value.

The β-NaYF$_4$:Tm,Yb system has been primarily studied as a NIR-to-blue upconverter.[1,47-49]

Figure 8 (upper panel) shows the *IQY* vs irradiance plots for the Tm^{3+} ^{1}D$_2$→^{3}F$_4$ (450 nm) and

^{1}G$_4$→^{3}H$_6$ (474 nm) emission in our β-NaYF$_4$: 0.5%Tm, 25%Yb @NaYF$_4$ core-shell and β-

NaYF$_4$:0.5%Tm, 25%Yb core nanocrystals. The lower panel of Figure 8 shows the *EF* values

for the two transitions. Unfortunately, it is difficult to find *IQY* data in the literature for these

emissions with which to compare our results. Page, et al report measured *IQY* values for a single

crystal of β-NaYF$_4$: 0.1%Tm, 35%Yb as a function of irradiance.[50] At an irradiance of 10

W/cm^2, they report a NIR-to-blue *IQY* of approximately 0.03%, which is certainly consistent

with our results for the core-shell sample, for which surface quenching is minimal. Quantitative

comparison is difficult, however, because of the difference in the doping concentrations, the

physical forms of the samples (nano vs macro), and because it is not clear as to whether the *IQY*

values of Page include the Tm^{3+}: ^{1}D$_2$→^{3}F$_4$ emission at 450 nm. However, the *IQY* for the 450

nm transition in our core-shell sample is small relative to that of the 475 nm emission, and,

whether the 450 nm transition is included or not, the *IQY* of the blue upconversion for our core-

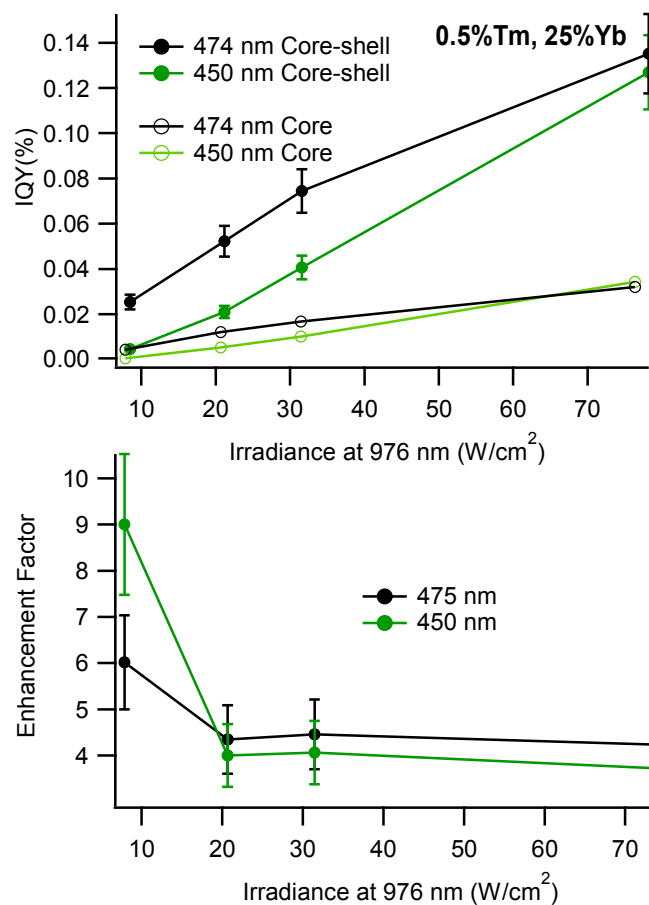shell sample at 10 W/cm^2 is quite close to the Page value of 0.03%.

Figure 8. (Upper panel) *IQY* vs irradiance plots for the Tm^{3+} $^1D_2\rightarrow^3F_4$ (450 nm) and $^1G_4\rightarrow^3H_6$ (475 nm) emission in β-NaYF$_4$: 0.5%Tm, 25%Yb @NaYF$_4$ core-shell nanocrystals. (Lower panel) Enhancement factors, *EF*, vs irradiance for the 475 nm and 450 nm emission, where

$$EF = \frac{IQY(core-shell)}{IQY(core)}.$$ The IQY error bars are the most probable error based on

assigning a 5% uncertainty value in each rate constant and integrated intensity value used to

calculate IQY. The resulting errors are 12% of the IQY value. The Enhancement Factor error

bars are the most probable error based on the 12% probable error in the core and core-shell IQY

values.

5. 2 Internal quantum yield of luminescence in β-NaYF$_4$: 2%Er, 18%Yb @ NaYF$_4$ core-shell and β-NaYF$_4$: 2%Er, 18%Yb core nanoparticles under cw excitation

5.2.1 Nanocrystal Size and Morphology

Figure 9 shows SEM images of the β-NaYF$_4$: 2%Er, 18%Yb nanocrystals before and after addition of a β-NaYF$_4$ shell.   The core nanocrystals are hexagonal prisms with an aspect ratio close to 1; the average edge-to-edge width across the hexagonal face is 55.9±3.1 nm and the length along the c-axis is 54.0±1.6 nm. Addition of the NaYF$_4$ shell to the core nanocrystals results in an increase in crystal size (width × length= 65.8±3.1 nm × 64.2±2.9 nm) and more pronounced hexagonal faceting. Therefore, the shell thickness for the core-shell nanocrystals is 5.1 nm on the axial (hexagonal) faces and 5.0 nm on the orthoaxial faces. The dimensions of the crystals are summarized in Table 3.
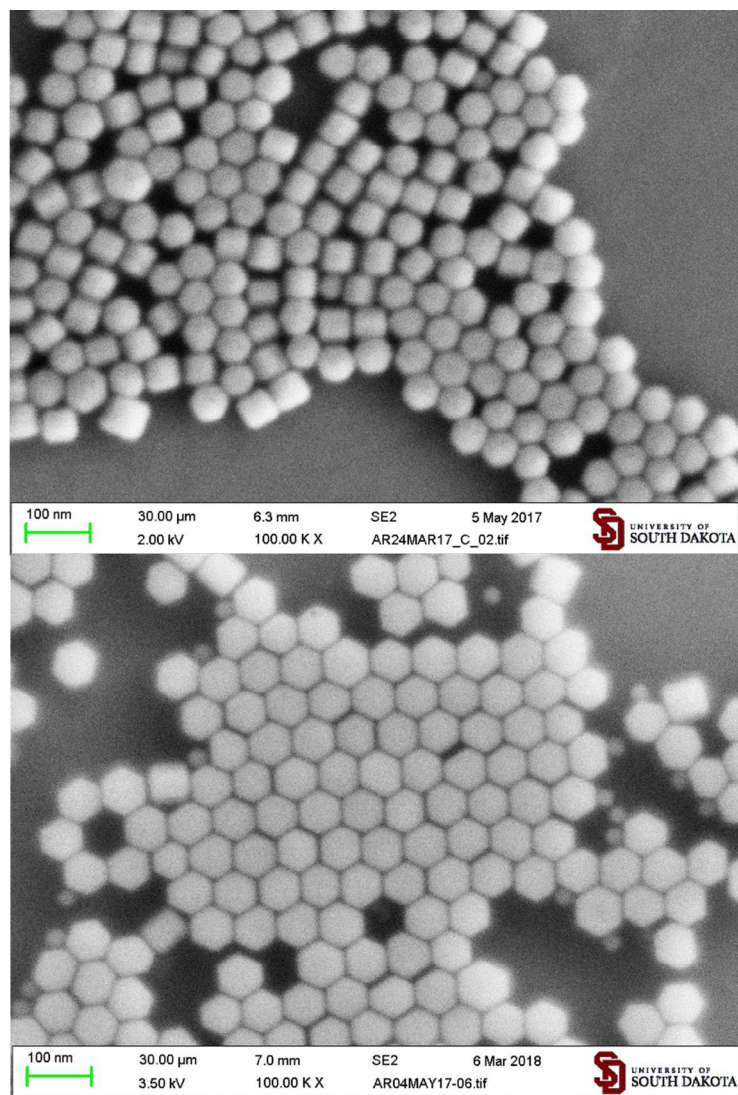
Figure 9. SEM images of β-NaYF$_4$: 2%Er, 18%Yb core (top panel) and β-NaYF$_4$: 2%Er, 18%Yb@NaYF$_4$ core-shell (bottom panel) nanocrystals. The dimensions of the crystals are summarized in Table 3.

Table 3. Dimensions of β-NaYF$_4$: 2%Er, 18%Yb core and β-NaYF$_4$: 2%Er, 18%Yb@NaYF$_4$ core-shell nanocrystals

Sample	Width (nm)	Length (nm)	Aspect ratio length/width	Ortho-face shell (nm)	Axial-face shell (nm)
β-NaYF$_4$: 2%Er, 18%Yb	55.9±3.1	54.0±1.6	0.97	---	---
β-NaYF$_4$: 2%Er, 18%Yb@NaYF$_4$	65.8±3.1	64.2±2.9	0.98	5.0	5.1

5.2.2 Upconversion and downshifted luminescence spectrum for β-NaYF$_4$: 2%Er, 18%Yb@NaYF$_4$ core-shell nanocrystals

Figure 10 shows the luminescence spectrum, in terms of δphotons/δλ vs λ, for β-NaYF$_4$: 2%Er, 18%Yb@NaYF$_4$ core-shell nanocrystals obtained using 936 nm excitation at 214 W/cm^2. This provides an excitation rate equivalent to 30.5 W/cm^2 at the Yb^{3+} absorbance maximum near 976 nm. The emission band at 1 μm is from Yb^{3+}; all other bands are assigned to Er^{3+}. Although the Er^{3+}:^{4}I$_{11/2}$→^{4}I$_{15/2}$ emission would also occur in the 1 μm range, the shape of the 1 μm curve in Figure 10 is not discernably different from that in the β-NaYF$_4$: 0.5%Tm, 25%Yb@NaYF$_4$ spectrum in Figure 3, for which Yb^{3+} is the only possible contributor to 1 μm emission. The 1 μm emission band in Figure 10 must, therefore, primarily be due to Yb^{3+} emission. As discussed

34

below, however, the equilibrium between Yb^{3+} and Er^{3+} at the 1 μm level does have an effect on the radiative decay constant for 1 μm emission.
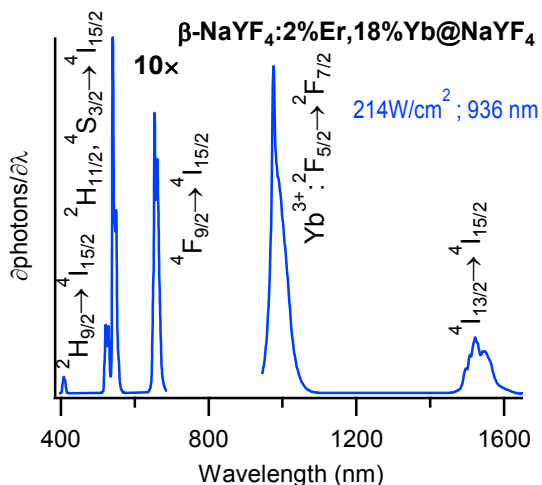

Figure 10. Corrected luminescence spectrum of β-NaYF$_4$: 2%Er, 18%Yb@NaYF$_4$ core-shell nanocrystals obtained using 936 nm excitation at 214 W/cm^2. This provides an excitation rate equivalent to 30.5 W/cm^2 at the Yb^{3+} absorbance maximum near 976 nm.

5.2.3 Determination of *IQY(1μm; low)* for β-NaYF$_4$: 2%Er, 18%Yb@NaYF$_4$ core-shell nanocrystals

Figure 11 shows the time dependence of 977 nm emission of Yb^{3+}/Er^{3+} for the core-shell and core sample following low-energy pulsed excitation at 950 nm, for which little or no UC emission was detectable. The curve for the core-shell sample fits well to an exponential function and the total decay rate at low excitation irradiance was determined to be $k_{tot}^{low}=682\pm1$ s^{-1}. Using our rate equations model,[15] the value of the radiative rate constant, k_{rad}, was estimated to be $k_{rad}=$

506 s^{-1}, so that, according to Equation 5, the internal quantum yield of the Yb^{3+} emission in the

'low power' region is $IQY(1\mu m; low) = \dfrac{k_{rad}}{k_{1\mu m}^{low}} = \dfrac{506 s^{-1}}{682 s^{-1}} = 0.742$. For the core sample, the curve

shape deviates significantly from an exponential function and $\int_0^\infty \dfrac{I(t)}{I(0)} dt = \left(k_{1\mu m}^{low} \right)^{-1} =$

$(3.755 \pm 0.141) \times 10^{-4}$ s, corresponding to $k_{1\mu m}^{low} = 2663 \pm 100$ s^{-1}. Therefore

$IQY(1\mu m; low) = \dfrac{k_{rad}}{k_{1\mu m}^{low}} = \dfrac{506 s^{-1}}{2663 s^{-1}} = 0.190$ for the core sample. These results are summarized in

Table 4. The value of k_{rad} is slightly lower than that given for the Yb, Tm system in Table 2,

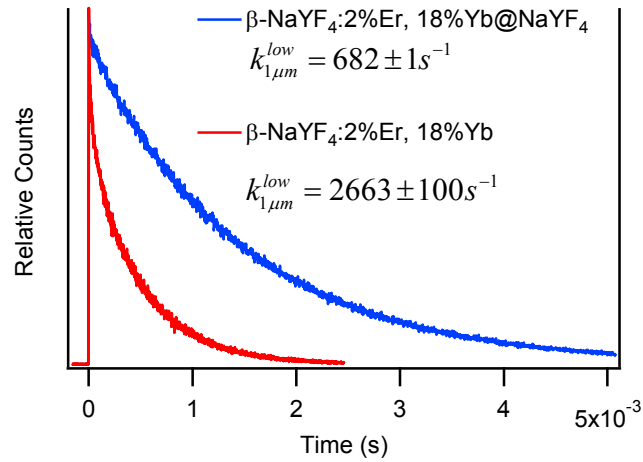because it is a weighted average of k_{rad} for Yb^{3+}(^{2}F$_{5/2}$) and Er^{3+}(^{4}I$_{11/2}$), which are in equilibrium.[15]

Figure 11. Time dependence of 977 nm emission of Yb^{3+} following pulsed excitation at 950 nm

for β-NaYF$_4$: 2%Er, 18%Yb@ NaYF$_4$ core-shell and β-NaYF$_4$: 2%Er, 18%Yb core nanocrystals.

The pulse-energy density used to acquire the decay curve was reduced until little or no UC

emission was detectable to ensure minimal contribution from non-linear processes.

Table 4. Inputs used to calculate the internal quantum yield for β-NaYF$_4$: 2%Er, 18%Yb@ NaYF$_4$ core-shell and β-NaYF$_4$: 2%Er, 18%Yb core nanocrystals in the limit of low excitation power/energy density.

Sample	k_{tot}^{low} (s^{-1})	k_{rad}(s^{-1})	$IQY_{1\mu m}^{low}$
Core-shell	682	506	0.742
Core	2663	506	0.190

5.2.4   Internal quantum yield, *IQY*, of β-NaYF$_4$: 2%Er, 18%Yb@ NaYF$_4$ core-shell and β-NaYF$_4$: 2%Er, 18%Yb core nanocrystals as a function of excitation irradiance

Corrected luminescence spectra (δphotons/δλ vs λ) for dispersions of the core-shell and core samples were measured for a series of excitation power densities under otherwise identical experimental conditions. Each series includes a spectrum of the 1 μm emission band acquired using excitation irradiance reduced to the point at which little or no upconversion could be observed.

The spectra were converted to represent $\partial(IQY)/\partial\lambda$ vs λ as described in Section 5.1.4, using the low-irradiance emission spectrum and the $IQY(1\mu m;low)$ value in Table 4 to determine the geometric constant, *C*.   The resulting $\partial(IQY)/\partial\lambda$ vs. λ spectra for the β-NaYF$_4$: 2%Er, 18%Yb@NaYF$_4$ core-shell sample are shown for three excitation-irradiance values in Figure 12.

As with the Tm^{3+}-activated system in the previous section, the $\partial(IQY)/\partial\lambda$ for upconversion emission in the Er^{3+} activated system increases with increasing irradiance while the $\partial(IQY)/\partial\lambda$ for the Yb^{3+} 1 μm emission decreases. The loss of 1 μm *IQY*, however, is much less pronounced than for the Tm^{3+}-activated UCNC, which is due to the less efficient upconversion in this system.
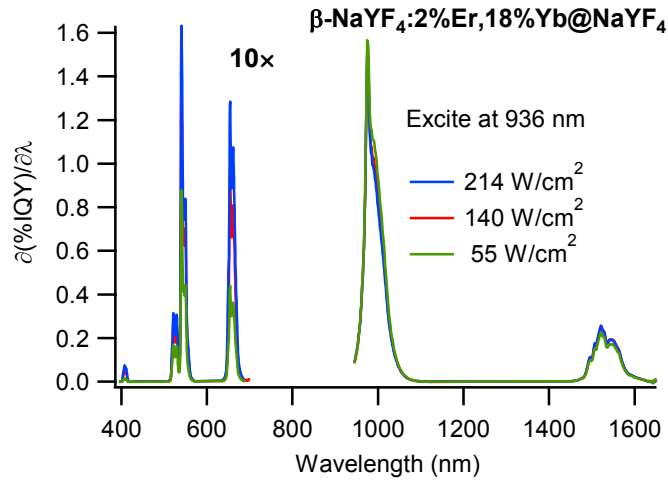

Figure 12. $\partial(IQY)/\partial\lambda$ vs. λ spectra of β-NaYF₄: 2%Er, 18%Yb@NaYF₄ core-shell nanocrystals dispersed in toluene using 936 nm excitation at irradiance values of 214, 140, and 55 W/cm². These irradiance values generate excitation rates equivalent to 30.5, 20, and 7.9 W/cm² at 976 nm. The $\partial(\%IQY)/\partial\lambda$ axis has quantitative meaning, in that the area under each emission band equals the corresponding internal quantum yield, *IQY(%)*, of that band.

The emission peaks in the $\partial(IQY)/\partial\lambda$ vs. λ spectra for the core-shell and core samples were then integrated to obtain the corresponding *IQY* values for the various luminescence transitions.

The upper panel of Figure 13 shows the core-shell and core *IQY* for the green (Er^{3+}: $^2H_{11/2}$, $^4S_{3/2}$

$\rightarrow^4I_{15/2}$) and red (Er^{3+}: $^4F_{9/2}$ $\rightarrow^4I_{15/2}$) upconversion emission, over the range of excitation

irradiance measured. The middle panel of Figure 13 shows the core-shell *IQY* vs. excitation

irradiance for the Yb^{3+}: $^2F_{5/2}\rightarrow^2F_{7/2}$ transition at 1 μm, the Er^{3+}: $^4I_{13/2}\rightarrow^4I_{15/2}$ transition at 1.5 μm,

and the sum of all emission from the sample, with each *IQY* value multiplied by the number of

photons required to reach the emitting state, $\sum IQY\ n(photons)$. The lower panel of Figure 13

shows the core *IQY* vs. excitation irradiance for the Yb^{3+}: $^2F_{5/2}\rightarrow^2F_{7/2}$ transition at 1 μm, the Er^{3+}:

$^4I_{13/2}\rightarrow^4I_{15/2}$ transition at 1.5 μm, and the sum of all emission from the sample, with each *IQY*

value multiplied by the number of photons required to reach the emitting state,

$\sum IQY\ n(photons)$. Although the actual excitation wavelength used in the experiments was

936 nm, the irradiance scale in Figure 13 has been corrected to the irradiance required to produce

an equivalent excitation rate near the Yb^{3+} absorbance maximum of 976 nm.
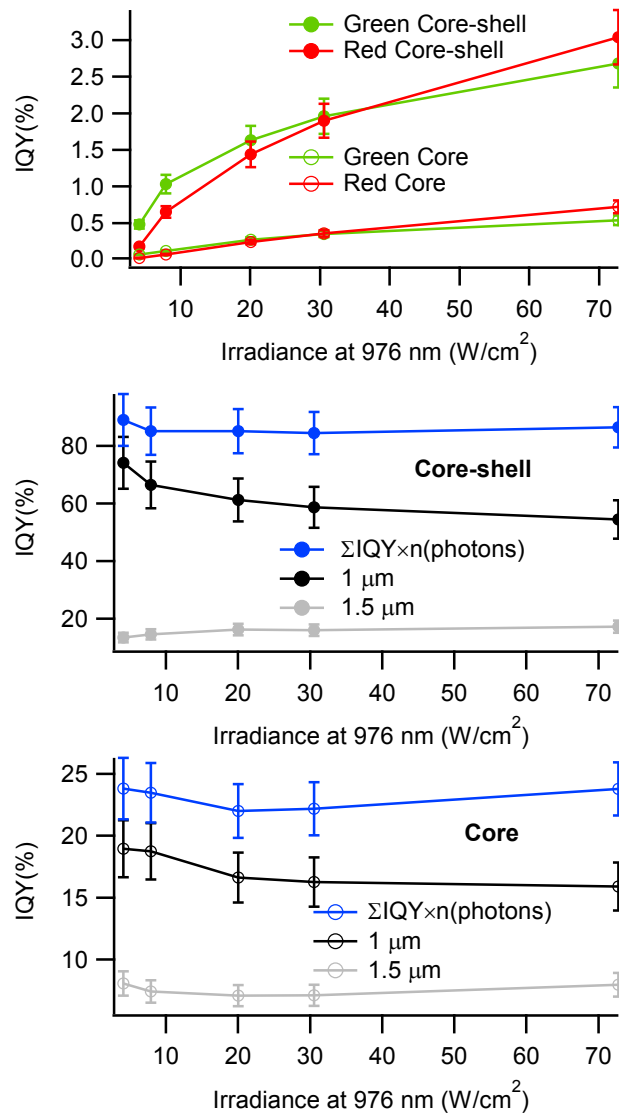
Figure 13. (Upper panel) Core-shell and core *IQY* for the green (Er^{3+}: $^2H_{11/2}$, $^4S_{3/2} \rightarrow ^4I_{15/2}$) and

red (Er^{3+}: $^4F_{9/2} \rightarrow ^4I_{15/2}$) upconversion emissions of β-NaYF$_4$: 2%Er, 18%Yb@NaYF$_4$ core-shell

and β-NaYF$_4$: 2%Er, 18%Yb@NaYF$_4$ core nanocrystals over the range of excitation power

densities measured. (Middle panel) Core-shell *IQY* vs. irradiance for the Yb^{3+}: $^2F_{5/2} \rightarrow ^2F_{7/2}$

transition at 1 μm, the Er^{3+}: $^4I_{13/2} \rightarrow ^4I_{15/2}$ transition at 1.5 μm, and the sum of all emission from

the sample, with each *IQY* value multiplied by the number of photons required to reach the

emitting state, $\sum IQY\, n(photons)$. (Lower panel) Core *IQY* vs. irradiance for the Yb^{3+}:

$^2F_{5/2} \rightarrow {}^2F_{7/2}$ transition at 1 μm, the Er^{3+}: $^4I_{13/2} \rightarrow {}^4I_{15/2}$ transition at 1.5 μm, and the sum of all emission from the sample, with each *IQY* value multiplied by the number of photons required to reach the emitting state, $\sum IQY\, n(photons)$. The irradiance scales have been corrected to the irradiance required to produce an equivalent excitation rate near the Yb^{3+} absorbance maximum of 976 nm. The error bars are the most probable error based on assigning a 5% uncertainty value in each rate constant and integrated intensity value used to calculate IQY. The resulting errors are 12% of the IQY value.

As was true for the Tm, Yb sample, the *IQY* vs irradiance plots for the 1 μm emission of Yb^{3+} for the core-shell and core samples (middle and lower panels of Figure 13) show that the increased *IQY* of the visible upconversion emission comes at the expense of the $Yb^{3+}(^2F_{5/2})$ excited-state population, with the *IQY* of the Yb^{3+} 1 μm emission dropping as the *IQY* of the green and red emission rises.

Also, as with the Tm, Yb sample, it is useful to correlate the behavior of the IQY for the upconversion and downshifted emission. The middle and lower panels of Figure 13 include plots of $\sum IQY\, n(photons)$, where *IQY n(photons)* is the IQY of a given emission multiplied by the order of the excitation process. The sum includes all upconversion and downshifted emission. These plots are relatively constant with excitation irradiance for both the core-shell and core samples, showing that the loss in *IQY*(1 μm) is almost quantitatively accounted for by the increases in upconversion emission.

Figure 14 shows the *EF* values for the upconversion and downshifted emission that accompany shell addition. As with the Tm, Yb system, the *EF* for the upconversion processes tend to

41

decrease with increasing irradiance, while the *EF* for the downshifted emissions remain relatively constant.   At low irradiance, the *EF* for upconversion emissions increase as green<red<blue. As irradiance increases, however, the differences in the *EF* become less pronounced, and even the ordering of the *EF* for the UC emissions changes.
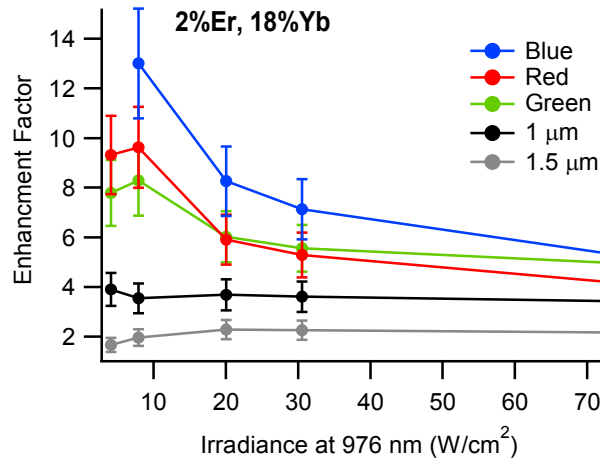

Figure 14.   Enhancement factors, *EF*, vs irradiance for the upconversion and downshifted luminescence of the 2%Er, 18%Yb system, where $EF = {IQY(core-shell)}/{IQY(core)}$. The error bars are the most probable error based on the 12% probable error in the core and core-shell IQY values.

Our rate-equations modeling of β-NaYF$_4$: Er, Yb nanosystems led us to the conclusion that the primary surface effect is the quenching of the energy reservoir at 1 μm, and that one could approximately predict the *IQY* behavior of any given β-NaYF$_4$: Er, Yb nanocrystal based on the value of $k_{1\mu m}^{low}$.[15] It was demonstrated that the model successfully predicted the IQY vs irradiance

behavior of Er, Yb systems reported in the literature.[15] Figure 15 compares the observed *IQY vs* irradiance plots for the red plus green upconversion (upper panel) and the blue upconversion (lower panel) for the β-NaYF$_4$: 2%Er, 18%Yb@ NaYF$_4$ core-shell and β-NaYF$_4$: 2%Er, 18%Yb core nanocrystals with the rate-equation simulated values for β-NaYF$_4$: 2%Er, 18%Yb materials with $k_{1\mu m}^{low}$ values of 610s^{-1}, 820 s^{-1}, 1176s^{-1}, 2439 s^{-1}, and 4762 s^{-1}. The blue upconversion corresponds to the Er^{3+}: ^{2}H$_{9/2}$→^{4}I$_{15/2}$ transition at 408 nm. The value of $k_{1\mu m}^{low} = 610$s^{-1} corresponds to that observed for the bulk material, so the corresponding plot in Figure 15 represents the upper limit of the *IQY* for β-NaYF$_4$: 2%Er, 18%Yb. Referring to the upper panel of Figure 15, the experimental red plus green IQY data for both the core-shell and core samples correlate closely to the simulated plots with similar $k_{1\mu m}^{low}$ values. The level of correspondence between our experimental results and the simulated predictions is quite good, and our experimental results are clearly consistent with the predictions of the rate equations model. Referring to the lower panel of Figure 15, the blue *IQY* data is reasonably consistent with the simulated predictions, except that the *IQY* values for the blue emission appear to plateau at lower irradiance than the simulations predict. The *IQY* of the blue upconversion is, however, very low, barely exceeding 0.1% at 70W/cm^2.
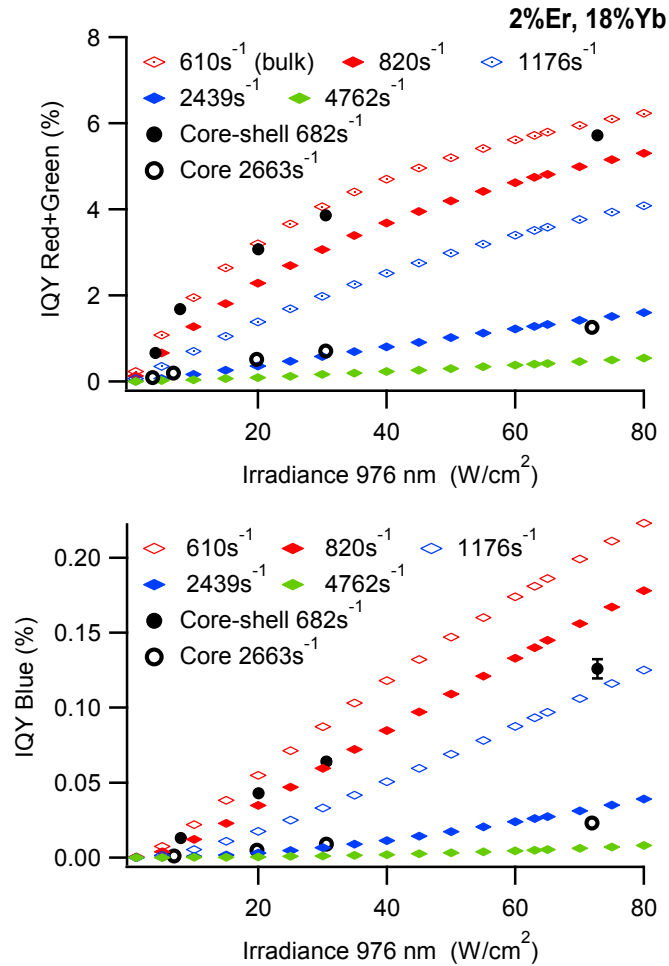
Figure 15. Comparison of observed *IQY vs* irradiance values for the red plus green upconversion (upper panel) and the blue upconversion (lower panel) for the β-NaYF$_4$: 2%Er, 18%Yb@ NaYF$_4$ core-shell and β-NaYF$_4$: 2%Er, 18%Yb core nanocrystals with the rate-equation simulated values for β-NaYF$_4$: 2%Er, 18%Yb materials with $k_{1\mu m}^{low}$ values of 610s^{-1}, 820 s^{-1}, 1176s^{-1}, 2439 s^{-1}, and 4762 s^{-1}. The blue upconversion corresponds to the Er^{3+}: $^2H_{9/2} \rightarrow {}^4I_{15/2}$ transition at 408 nm. Diamond symbols represent the simulated values. Closed black circles represent the experimental values for the core-shell sample. Open black circles represent the experimental values for the core sample.

Direct comparison of the measured *IQY* for our core-shell system to other values reported in the literature is problematic, because it is difficult to account for the variations in surface quenching in the different samples if investigators do not report the decay rate constant for the 1 μm emission, which is so useful in comparing quenching effects. Page, et al report that the limiting *IQY* for green upconversion in bulk β-NaYF$_4$: 2%Er, 18%Yb is 4%.[50]   Boyer, et al report the green upconversion *IQY* in microcrystals of β-NaYF$_4$: 2%Er, 18%Yb to be 3% at 20 W/cm^2.[20] Kaiser et al report that the maximum green *IQY* in 3μm-sized β-NaYF$_4$: 2.2%Er, 21.4%Yb crystals is 2.4% at 20 W/cm^2.[30]   Our results shown in Figure 13 are certainly consistent with these values, given that the present core-shell nanocrystals should have *IQY* lower than the bulk, but not dramatically lower.

The *IQY* data on 3μm-sized β-NaYF$_4$: 2.2%Er, 21.4%Yb crystals in the Kaiser study[30] provides a useful reference point with which to compare our current results. Their *IQY* vs irradiance data indicate that the crossing point where the *IQY* of the red and green UC are equal is

$IQY(red) = IQY(green) \approx 2\%$, which is very similar to that observed for our β-NaYF$_4$: 2%Er, 18%Yb@NaYF$_4$ core-shell nanocrystals. (See Figure 13, upper panel.)   We note, however, that, for the micron-sized crystals, the crossing point occurs at an irradiance of ~11W/cm^2,[30] whereas, for our transparent core-shell dispersions, the crossing point is observed at ~30W/cm^2. We attribute the observed shift in the crossing-point irradiance to the fact that scattering in powder samples increases the effective excitation irradiance in the sample, such that the effective irradiance of the Kaiser powders is significantly higher than the incidence irradiance of 11W/cm^2. In our previous studies of densely-packed microcrystalline powders of β-NaYF$_4$: 2%Er, 18%Yb, we estimated that the effective pulse-energy density in the sample is ~3× that of

the incident pulse-energy density.[15] The issue of irradiance distortion by scattering samples was also noted by Page in his study,[50] although he does not attempt to quantify it.

6. Conclusions

A new method, using an internal standard, for the determination of internal quantum yields (IQY) vs irradiance (or pulse-energy density) for Yb-sensitized energy-transfer upconversion materials has been presented and demonstrated to be consistent with direct determination methods and numerical simulations. For the two systems studied here, the IQY vs irradiance for both the upconversion and downshifted luminescence was determined. Correlation of the IQY of the upconversion and downshifted emission served as a useful check of the internal consistency of our results, and provided valuable insight into the photo-physics of the systems.

The first major advantage to this method of internal standards is that it should be accessible to large number of research labs currently investigating upconversion materials. This could significantly benefit the research community if it results in more widespread reporting of the IQY behavior of the upconversion nanocrystals (UCNC) being studied; it would enable more reliable correlation of reported results with the intrinsic photo-physical properties of materials used. The second advantage is that the method does not rely on the sample exhibiting measurable absorbance of the excitation source. This will enable the acquisition of IQY data on a much wider range of samples in their intended-application environment (e.g., thin films, dilute dispersions, aqueous dispersions).

We are currently investigating whether similar methods can be extended to Nd^{3+}-sensitized upconversion phosphors.

Conflicts of interest

There are no conflicts to declare.

Acknowledgements

Notes and references

(1)   Heer, S.; Kömpe, K.; Güdel, H. U.; Haase, M. Highly Efficient Multicolour Upconversion Emission in Transparent Colloids of Lanthanide-Doped $NaYF_4$ Nanocrystals. *Adv. Mater.* **2004**, *16*, 2102.

(2)   Yi, G.; Lu, H.; Zhao, S.; Ge, Y.; Yang, W.; Chen, D.; Guo, L.-H. Synthesis, Characterization, and Biological Application of Size-Controlled Nanocrystalline $NaYF_4$:Yb,Er Infrared-to-Visible Up-Conversion Phosphors. *Nano Lett.* **2004**, *4*, 2191-2196.

(3)   Zhou, J.; Liu, Q.; Feng, W.; Sun, Y.; Li, F. Upconversion Luminescent Materials: Advances and Applications. *Chem Rev* **2015**, *115*, 395-465.

(4)   Chen, G.; Agren, H.; Ohulchanskyy, T. Y.; Prasad, P. N. Light upconverting core-shell nanostructures: nanophotonic control for emerging applications. *Chem Soc Rev* **2015**, *44*, 1680-1713.

(5)   Wu, D. M.; García-Etxarri, A.; Salleo, A.; Dionne, J. A. Plasmon-Enhanced Upconversion. *J. Phys. Chem. Lett.* **2014**, *5*, 4020-4031.

(6)   Han, S.; Deng, R.; Xie, X.; Liu, X. Enhancing Luminescence in Lanthanide-Doped Upconversion Nanoparticles. *Angew Chem Int Edit* **2014**, *53*, 11702-11715.

(7)   Chen, G.; Qiu, H.; Prasad, P. N.; Chen, X. Upconversion Nanoparticles: Design, Nanochemistry, and Applications in Theranostics. *Chem Rev* **2014**, *114*, 5161-5214.

(8)   Haase, M.; Schäfer, H. Upconverting Nanoparticles. *Angew. Chem. Int. Ed.* **2011**, *50*, 5808-5829.

(9)   Kumar, P.; Singh, S.; Gupta, B. K. Future prospects of luminescent nanomaterial based security inks: from synthesis to anti-counterfeiting applications. *Nanoscale* **2016**, *8*, 14297-14340.

(10)   Liu, X.; Yan, C.-H.; Capobianco, J. A. Photon upconversion nanomaterials. *Chem Soc Rev* **2015**, *44*, 1299-1301.

(11)   van der Ende, B. M.; Aarts, L.; Meijerink, A. Lanthanide ions as spectral converters for solar cells. *Phys. Chem. Chem. Phys.* **2009**, *11*, 11081-11095.

(12)   Zheng, W.; Huang, P.; Tu, D.; Ma, E.; Zhu, H.; Chen, X. Lanthanide-doped upconversion nano-bioprobes: electronic structures, optical properties, and biodetection. *Chem Soc Rev* **2015**, *44*, 1379-1415.

(13)   Zhou, B.; Shi, B.; Jin, D.; Liu, X. Controlling upconversion nanocrystals for emerging applications. *Nat Nano* **2015**, *10*, 924-936.

(14)   Goldschmidt, J. C.; Fischer, S. Upconversion for Photovoltaics − a Review of Materials, Devices and Concepts for Performance Enhancement. *Advanced Optical Materials* **2015**, *3*, 510-535.

(15)   Hossan, M. Y.; Hor, A.; Luu, Q.; Smith, S. J.; May, P. S.; Berry, M. T. Explaining the Nanoscale Effect in the Upconversion Dynamics of β-NaYF$_4$:Yb^{3+}, Er^{3+} Core and Core–Shell Nanocrystals. *J. Phys. Chem. C* **2017**, *121*, 16592-16606.

(16)   Fischer, S.; Bronstein, N. D.; Swabeck, J. K.; Chan, E. M.; Alivisatos, A. P. Precise Tuning of Surface Quenching for Luminescence Enhancement in Core–Shell Lanthanide-Doped Nanocrystals. *Nano Letters* **2016**, *16*, 7241-7247.

(17)   Fisher, J.; Zhao, B.; Lin, C.; Berry, M.; May, P. S.; Smith, S. Spectroscopic Imaging and Power Dependence of Near-Infrared to Visible Upconversion Luminescence from NaYF$_4$:Yb^{3+},Er^{3+} Nanoparticles on Nanocavity Arrays. *J. Phys. Chem. C* **2015**, *119*, 24976-24982.

(18)   Zhao, J.; Jin, D.; Schartner, E. P.; Lu, Y.; Liu, Y.; Zvyagin, A. V.; Zhang, L.; Dawes, J. M.; Xi, P.; Piper, J. A.; Goldys, E. M.; Monro, T. M. Single-nanocrystal sensitivity achieved by enhanced upconversion luminescence. *Nat Nano* **2013**, *8*, 729-734.

(19)   Fischer, S.; Fröhlich, B.; Krämer, K. W.; Goldschmidt, J. C. Relation between Excitation Power Density and Er3+ Doping Yielding the Highest Absolute Upconversion Quantum Yield. *J Phys Chem C* **2014**, *118*, 30106-30114.

(20)   Boyer, J.-C.; van Veggel, F. C. J. M. Absolute Quantum Yield Measurements of Colloidal NaYF$_4$: Er^{3+}, Yb^{3+} Upconverting Nanoparticles. *Nanoscale* **2010**, *2*, 1417-1419.

(21)   Chen, G.; Ohulchanskyy, T. Y.; Kachynski, A.; Ågren, H.; Prasad, P. N. Intense Visible and Near-Infrared Upconversion Photoluminescence in Colloidal LiYF4:Er3+ Nanocrystals under Excitation at 1490 nm. *ACS Nano* **2011**, *5*, 4981-4986.

(22)   Liu, Q.; Sun, Y.; Yang, T.; Feng, W.; Li, C.; Li, F. Sub-10 nm Hexagonal Lanthanide-Doped NaLuF$_4$ Upconversion Nanocrystals for Sensitive Bioimaging in Vivo. *J Am Chem Soc* **2011**, *133*, 17122-17125.

(23)   Chen, G.; Shen, J.; Ohulchanskyy, T. Y.; Patel, N. J.; Kutikov, A.; Li, Z.; Song, J.; Pandey, R. K.; Ågren, H.; Prasad, P. N.; Han, G. (α-NaYbF$_4$:Tm^{3+})/CaF$_2$ Core/Shell Nanoparticles with Efficient Near-Infrared to Near-Infrared Upconversion for High-Contrast Deep Tissue Bioimaging. *ACS Nano* **2012**, *6*, 8280-8287.

(24)   Faulkner, D. O.; Petrov, S.; Perovic, D. D.; Kherani, N. P.; Ozin, G. A. Absolute quantum yields in NaYF$_4$:Er,Yb upconverters - synthesis temperature and power dependence. *J Mater Chem* **2012**, *22*, 24330-24334.

(25)   Ostrowski, A. D.; Chan, E. M.; Gargas, D. J.; Katz, E. M.; Han, G.; Schuck, P. J.; Milliron, D. J.; Cohen, B. E. Controlled Synthesis and Single-Particle Imaging of Bright, Sub-10 nm Lanthanide-Doped Upconverting Nanocrystals. *ACS Nano* **2012**, *6*, 2686-2692.

(26)   Xu, C. T.; Svenmarker, P.; Liu, H.; Wu, X.; Messing, M. E.; Wallenberg, L. R.; Andersson-Engels, S. High-Resolution Fluorescence Diffuse Optical Tomography Developed with Nonlinear Upconverting Nanoparticles. *ACS Nano* **2012**, *6*, 4788-4795.

(27)   Liu, H.; Xu, C. T.; Lindgren, D.; Xie, H.; Thomas, D.; Gundlach, C.; Andersson-Engels, S. Balancing power density based quantum yield characterization of upconverting nanoparticles for arbitrary excitation intensities. *Nanoscale* **2013**, *5*, 4770-4775.

(28)   Shen, J.; Chen, G.; Ohulchanskyy, T. Y.; Kesseli, S. J.; Buchholz, S.; Li, Z.; Prasad, P. N.; Han, G. Tunable Near Infrared to Ultraviolet Upconversion Luminescence Enhancement in (α-NaYF$_4$:Yb,Tm)/CaF$_2$ Core/Shell Nanoparticles for In situ Real-time Recorded Biocompatible Photoactivation. *Small* **2013**, *9*, 3213-3217.

(29)   Li, X.; Wang, R.; Zhang, F.; Zhao, D. Engineering homogeneous doping in single nanoparticle to enhance upconversion efficiency. *Nano letters* **2014**, *14*, 3634-3639.

(30)   Kaiser, M.; Wurth, C.; Kraft, M.; Hyppanen, I.; Soukka, T.; Resch-Genger, U. Power-dependent upconversion quantum yield of NaYF$_4$:Yb^{3+},Er^{3+} nano- and micrometer-sized particles - measurements and simulations. *Nanoscale* **2017**, *9*, 10051-10058.

(31)   Wurth, C.; Kaiser, M.; Wilhelm, S.; Grauel, B.; Hirsch, T.; Resch-Genger, U. Excitation power dependent population pathways and absolute quantum yields of upconversion nanoparticles in different solvents. *Nanoscale* **2017**, *9*, 4283-4294.

(32)   Würth, C.; Fischer, S.; Grauel, B.; Alivisatos, A. P.; Resch-Genger, U. Quantum Yields, Surface Quenching, and Passivation Efficiency for Ultrasmall Core/Shell Upconverting Nanoparticles. *J Am Chem Soc* **2018**, *140*, 4922-4928.

(33)   Homann, C.; Krukewitt, L.; Frenzel, F.; Grauel, B.; Wurth, C.; Resch-Genger, U.; Haase, M. NaYF4 :Yb,Er/NaYF4 Core/Shell Nanocrystals with High Upconversion Luminescence Quantum Yield. *Angew Chem Int Ed Engl* **2018**, *57*, 1-6.

(34)   Fischer, S.; Fröhlich, B.; Steinkemper, H.; Krämer, K. W.; Goldschmidt, J. C. Absolute upconversion quantum yield of β-NaYF$_4$ doped with Er^{3+} and external quantum efficiency of upconverter solar cell devices under broad-band excitation considering spectral mismatch corrections. *Sol Energ Mat Sol C* **2014**, *122*, 197-207.

(35)   Luu, Q.; Hor, A.; Fisher, J.; Anderson, R. B.; Liu, S.; Luk, T. S.; Paudel, H. P.; Baroughi, M. F.; May, P. S.; Smith, S. Two-Color Surface Plasmon Polariton Enhanced Upconversion in NaYF4:Yb:Tm Nanoparticles on Au Nanopillar Arrays. *J Phys Chem C* **2014**, *118*, 3251-3257.

(36)   Paudel, H. P.; Zhong, L.; Bayat, K.; Baroughi, M. F.; Smith, S.; Lin, C.; Jiang, C.; Berry, M. T.; May, P. S. Enhancement of Near-Infrared-to-Visible Upconversion Luminescence Using Engineered Plasmonic Gold Surfaces. *J. Phys. Chem. C* **2011**, *115*, 19028-19036.

(37)   Fischer, S.; Swabeck, J. K.; Alivisatos, A. P. Controlled Isotropic and Anisotropic Shell Growth in β-NaLnF$_4$ Nanocrystals Induced by Precursor Injection Rate. *J Am Chem Soc* **2017**, *139*, 12325-12332.

(38)   Inokuti, M.; Hirayama, F. Influence of Energy Transfer by the Exchange Mechanism on Donor Luminescence. *J. Chem. Phys.* **1965**, *43*, 1978-1989.

(39)   DeLoach, L. D.; Payne, S. A.; Chase, L. L.; Smith, L. K.; Kway, W. L.; Krupke, W. F. Evaluation of absorption and emission properties of Yb^{3+} doped crystals for laser applications. *IEEE Journal of Quantum Electronics* **1993**, *29*, 1179-1191.

(40)   Strickler, S. J.; Berg, R. A. Relationship between Absorption Intensity and Fluorescence Lifetime of Molecules. *J Chem Phys* **1962**, *37*, 814-822.

(41)   Senden, T.; Rabouw, F. T.; Meijerink, A. Photonic Effects on the Radiative Decay Rate and Luminescence Quantum Yield of Doped Nanocrystals. *ACS Nano* **2015**, *9*, 1801-1808.

(42)   Qian, H.-S.; Zhang, Y. Synthesis of Hexagonal-Phase Core−Shell $NaYF_4$ Nanocrystals with Tunable Upconversion Fluorescence. *Langmuir* **2008**, *24*, 12123.

(43)   Li, Z.; Yong, Z. An Efficient and User-Friendly Method for the Synthesis of Hexagonal-Phase $NaYF_4$:Yb, Er/Tm Nanocrystals With Controllable Shape and Upconversion Fluorescence. *Nanotechnology* **2008**, *19*, 345606.

(44)   Johnson, N. J. J.; Korinek, A.; Dong, C.; van Veggel, F. C. J. M. Self-Focusing by Ostwald Ripening: A Strategy for Layer-by-Layer Epitaxial Growth on Upconverting Nanocrystals. *J. Am. Chem. Soc.* **2012**, *134*, 11068-11071.

(45)   Suter, J. D.; Pekas, N. J.; Berry, M. T.; May, P. S. Real-Time-Monitoring of the Synthesis of β-$NaYF_4$:17% Yb,3% Er Nanocrystals Using NIR-to-Visible Upconversion Luminescence. *J. Phys. Chem. C* **2014**, *118*, 13238-13247.

(46)   May, P. B.; Suter, J. D.; May, P. S.; Berry, M. T. The Dynamics of Nanoparticle Growth and Phase Change During Synthesis of β-$NaYF_4$. *J. Phys. Chem. C* **2016**, *120*, 9482-9489.

(47)   Krämer, K. W.; Biner, D.; Frei, G.; Güdel, H. U.; Hehlen, M. P.; Luthi, S. R. Hexagonal Sodium Yttrium Fluoride Based Green and Blue Emitting Upconversion Phosphors. *Chem. Mater.* **2004**, *16*, 1244.

(48)   Boyer, J.-C.; Vetrone, F.; Cuccia, L. A.; Capobianco, J. A. Synthesis of Colloidal Upconverting $NaYF_4$ Nanocrystals Doped with Er^{3+}, Yb^{3+} and Tm^{3+}, Yb^{3+} via Thermal Decomposition of Lanthanide Trifluoroacetate Precursors. *J. Am. Chem. Soc.* **2006**, *128*, 7444.

(49)   Suyver, J. F.; Aebischer, A.; Biner, D.; Gerner, P.; Grimm, J.; Heer, S.; Kramer, K. W.; Reinhard, C.; Güdel, H. U. Novel Materials Doped With Trivalent Lanthanides and Transition Metal Ions Showing Near-Infrared to Visible Photon Upconversion. *Opt. Mater.* **2005**, *27*, 1111.

(50)   Page, R. H.; Schaffers, K. I.; Waide, P. A.; Tassano, J. B.; Payne, S. A.; Krupke, W. F.; Bischel, W. K. Upconversion-pumped luminescence efficiency of rare-earth-doped hosts sensitized with trivalent ytterbium. *J Opt Soc Am B* **1998**, *15*, 996-1008.

TOC Entry: A new method is presented for estimating the internal quantum yield (*IQY*) of upconversion (UC) luminescence for Yb^{3+}-sensitized ETU phosphors.

β-NaYF₄:0.5%Tm, 25%Yb@NaYF₄ core-shell